Eur. Phys. J. C (2017) 77:502
DOI 10.1140/epjc/s10052-017-5069-1

THE EUROPEAN PHYSICAL JOURNAL C

Regular Article - Theoretical Physics

New observational constraints on $f(T)$ cosmology from radio quasars

Jing-Zhao Qi[1], **Shuo Cao**[1,a], **Marek Biesiada**[1,2], **Xiaogang Zheng**[1,2], **Zong-Hong Zhu**[1]

[1] Department of Astronomy, Beijing Normal University, Beijing 100875, China
[2] Department of Astrophysics and Cosmology, Institute of Physics, University of Silesia, Uniwersytecka 4, 40-007 Katowice, Poland

Received: 11 May 2017 / Accepted: 13 July 2017 / Published online: 28 July 2017

Abstract Using a new recently compiled milliarcsecond compact radio data set of 120 intermediate-luminosity quasars in the redshift range $0.46 < z < 2.76$, whose statistical linear sizes show negligible dependence on redshifts and intrinsic luminosity and thus represent standard rulers in cosmology, we constrain three viable and most popular $f(T)$ gravity models, where T is the torsion scalar in teleparallel gravity. Our analysis reveals that constraining power of the quasars data ($N = 120$) is comparable to the Union2.1 SN Ia data ($N = 580$) for all three $f(T)$ models. Together with other standard ruler probes such as cosmic microwave background and baryon acoustic oscillation distance measurements, the present value of the matter density parameter $\Omega_{\rm m}$ obtained by quasars is much larger than that derived from other observations. For one of the models considered (f_1CDM) a small but noticeable deviation from ΛCDM cosmology is present, while in the framework of f_3CDM the effective equation of state may cross the phantom divide line at lower redshifts. These results indicate that intermediate-luminosity quasars could provide an effective observational probe comparable to SN Ia at much higher redshifts, and $f(T)$ gravity is a reasonable candidate for the modified gravity theory.

1 Introduction

The current cosmic acceleration has been supported by many independent astrophysical observations, including type Ia supernovae (SN Ia) [1], large-scale structure [2], cosmic microwave background (CMB) anisotropy [3], etc. A mysterious component with negative pressure, dubbed dark energy, has been proposed to explain this phenomenon in the framework of Einstein's general relativity, which gave birth to a large number of dark energy models including the cosmological constant (ΛCDM), scalar field theory [4–6], and dynamical dark energy models [7–11]. The other direction one could follow in search for solution of the accelerating cosmic expansion enigma is to construct modified theories of gravity instead of invoking exotic dark energy. A large majority of works in this direction concentrated on the brane-world Dvali–Gabadadze–Porrati (DGP) model [12], $f(R)$ gravity [13], and Gauss–Bonnet gravity [14].

Equally well, one can also modify the gravity according to the scenario described by the so-called $f(T)$ theory [15], which was proposed in the framework of the Teleparallel Equivalent of General Relativity (also known as Teleparallel Gravity). In this approach, the Levi-Civita connection used in Einstein's general relativity is replaced by the Weitzenböck connection with torsion, while the Lagrangian density of this theory is the torsion scalar T. Compared with the $f(R)$ theory leading to the fourth order equations, the field equations of the $f(T)$ theory are in the form of second order differential equations, which provides an important advantage of this approach. In addition, if certain conditions are satisfied, the behavior of $f(T)$ cosmologies is similar to several popular dark energy models, such as quintessence [16], phantom [17], DGP model [18] and transient acceleration [19]. Due to the above mentioned property, $f(T)$ theory and its cosmological applications has gained a lot interest in the literature. A detailed introduction to the $f(T)$ theory could be found in [18,20].

In this paper, we focus on using the currently released quasar data [21] to provide the constraints on various $f(T)$ gravity models. Recently, the angular size of compact structure in radio quasars versus redshift data from the very-long-baseline interferometry (VLBI) observations have become an effective probe in cosmology. Reliable standard rulers and standard candles at cosmological scales are crucial for measuring cosmic distances at different redshifts. For instance, the type Ia supernovae are regarded as standard candles, while the BAO peak location is commonly recognized as a fixed

[a] e-mail: caoshuo@bnu.edu.cn

comoving ruler. The increasing observational material concerning these two distance indicators has been widely used in various cosmological studies. In the past, there were controversial discussions about whether the compact radio sources could act as standard rulers [22–26]. The difficulty lies in the fact that the linear sizes l_m of compact radio sources might not be constant, i.e., its value is dependent on both redshifts and some intrinsic properties of the source (luminosity, for example). Based on a 2.29 GHz VLBI all-sky survey of 613 milliarcsecond ultra-compact radio sources [27,28], Cao et al. [21] presented a method to divide the full sample into different sub-samples, according to their optical counterparts and luminosity (low-luminosity quasars, intermediate-luminosity quasars, and high-luminosity quasars). The final results indicated that intermediate-luminosity quasars show negligible dependence on both redshifts z and intrinsic luminosity L, which makes them a fixed comoving-length standard ruler. More recently, based on a cosmological-model-independent method to calibrate the linear sizes l_m of intermediate-luminosity quasars, Cao et al. [29] investigated the cosmological application of this data set and obtained stringent constraints on both the matter density $\Omega_{\rm m}$ and the Hubble constant H_0, which agree very well with the recent *Planck* results. The advantage of this data set, compared with other standard rulers, BAO [30–32], clusters [33], strong lensing systems [34–36]), is that quasars are observed at much higher redshifts ($z \sim 3.0$). Therefore, it may be rewarding to test the $f(T)$ theory with this newly revised quasar data. In this paper, we examine constraints on the viable $f(T)$ cosmological models imposed by the quasars. We compare them with analogous results obtained with the newly revised Union2.1 set—the largest published and spectroscopically confirmed SN Ia sample to date. We expect that different systematics and sensitivities of these two different probes (rulers vs. candles) can give complementary results on the $f(T)$ theory.

This paper is organized as follows: In Sect. 2 we briefly introduce the $f(T)$ gravity and its cosmological consequences. In Sect. 3 we present the latest data sets for our analysis and perform a Markov chain Monte Carlo analysis using different data sets in Sect. 4. Finally, we summarize the main conclusions in Sect. 5.

2 The $f(T)$ theory

In this section we brief review the $f(T)$ gravity in the framework of cosmology, and then we present three specific $f(T)$ models to be analyzed in this work.

2.1 The $f(T)$ cosmology

We use the vierbein fields $\mathbf{e}_i(x^\mu)$ ($i = 0, 1, 2, 3$), which is an orthonormal basis for the tangent space at each point x^μ of the manifold $\mathbf{e}_i \cdot \mathbf{e}_j = \eta_{ij}$, and whose components are e_i^μ ($\mu = 0, 1, 2, 3$) (here Latin indices stand for the tangent space and Greek indices refer to the manifold). Its dual vierbein gives the metric tensor $g_{\mu\nu}(x) = \eta_{ij}\, e_\mu^i(x)\, e_\nu^j(x)$. In $f(T)$ theory, instead of the torsionless Levi-Civita connection in Einstein's General Relativity, the curvatureless Weitzenböck connection is considered, and hence the torsion tensor describing the gravitational field is

$$T^\lambda_{\mu\nu} \equiv e_i^\lambda(\partial_\mu e_\nu^i - \partial_\nu e_\mu^i). \tag{1}$$

The Lagrangian of teleparallel gravity is constructed by the torsion scalar as [15]

$$T \equiv S_\rho^{\mu\nu}\, T^\rho_{\mu\nu}, \tag{2}$$

where

$$S_\rho^{\mu\nu} = \frac{1}{2}\Big(K_\rho^{\mu\nu} + \delta_\rho^\mu T_\theta^{\theta\nu} - \delta_\rho^\nu T_\theta^{\theta\mu}\Big), \tag{3}$$

and the contorsion tensor $K_\rho^{\mu\nu}$ is given by

$$K_\rho^{\mu\nu} = -\frac{1}{2}\Big(T_\rho^{\mu\nu} - T_\rho^{\nu\mu} - T_\rho^{\mu\nu}\Big). \tag{4}$$

In the $f(T)$ theory, the Lagrangian density is a function of T [15], and the action reads

$$I = \frac{1}{16\pi G}\int \mathrm{d}^4x\, e\, f(T), \tag{5}$$

where $e = \det(e_\mu^i) = \sqrt{-g}$. The corresponding field equation is

$$\begin{aligned}&[e^{-1}\partial_\mu(eS_i^{\mu\nu}) - e_i^\lambda\, T^\rho_{\mu\lambda}S_\rho^{\nu\mu}]f_T\\ &\quad + S_i^{\mu\nu}\partial_\mu T f_{TT} + \frac{1}{4}e_i^\nu f(T) = \frac{1}{2}k^2 e_i^\rho T_\rho^\nu,\end{aligned} \tag{6}$$

where $k^2 = 8\pi G$, $f_T \equiv \mathrm{d}f/\mathrm{d}T$, $f_{TT} \equiv \mathrm{d}^2 f/\mathrm{d}T^2$, $S_i^{\mu\nu} \equiv e_i^\rho S_\rho^{\mu\nu}$, and $T_{\mu\nu}$ is the matter energy-momentum tensor. Considering a flat homogeneous and isotropic FRW Universe, we have

$$\begin{aligned}e_\mu^i &= \mathrm{diag}\,(1, a(t), a(t), a(t))\,,\\ e_i^\mu &= \mathrm{diag}\left(1, \frac{1}{a(t)}, \frac{1}{a(t)}, \frac{1}{a(t)}\right),\end{aligned} \tag{7}$$

where $a(t)$ is the cosmological scale factor. By substituting Eqs. (7), (1), (3) and (4) into Eq. (2), one could obtain the torsion scalar as [15]

$$T \equiv S^{\rho\mu\nu}T_{\rho\mu\nu} = -6H^2, \tag{8}$$

where H is the Hubble parameter $H = \dot{a}/a$. The dot represents the first derivative with respect to the cosmic time.

Substituting Eq. (7) into (6), one can obtain the corresponding Friedmann equations

$$12H^2 f_T + f = 2k^2\rho, \tag{9}$$
$$48H^2\dot{H} f_{TT} - (12H^2 + 4\dot{H}) f_T - f = 2k^2 p, \tag{10}$$

where ρ and p are the total energy density and pressure, respectively. By defining the effective energy density $\rho_{\rm eff}$, pressure $p_{\rm eff}$ and effective equation of state (EoS) parameter $w_{\rm eff}$ as

$$\rho_{\rm eff} = \frac{1}{2k^2}(-12H^2 f_T - f + 6H^2), \tag{11}$$
$$p_{\rm eff} = -\frac{1}{2k^2}[48\dot{H}H^2 f_{TT} - 4\dot{H} f_T + 4\dot{H}] - \rho_{\rm eff}, \tag{12}$$
$$w_{\rm eff} = -\frac{f/T - f_T + 2T f_{TT}}{[1 + f_T + 2T f_{TT}][f/T - 2f_T]}. \tag{13}$$

The Friedmann equations could be rewrite as

$$\frac{3}{k^2}H^2 = \rho + \rho_{\rm eff}, \tag{14}$$
$$\frac{1}{k^2}(2\dot{H} + 3H^2) = -(p + p_{\rm eff}). \tag{15}$$

Therefore, the cosmic acceleration could be driven by the torsion instead of dark energy. In this cosmological framework, the corresponding normalized Hubble parameter is

$$E^2(z) \equiv \frac{H^2(z)}{H_0^2} = \frac{T(z)}{T_0}, \tag{16}$$

where $T_0 = -6H_0^2$ (the subscript "0" denotes the current value). Here we consider the matter and radiation in the Universe—the components whose energy density evolves with redshift z as $\rho_m = \rho_{m0}(1+z)^3$, $\rho_r = \rho_{r0}(1+z)^4$, respectively. Then Eq. (16) could be expressed as [37,38]

$$E^2(z, \mathbf{p}) = \Omega_m(1+z)^3 + \Omega_r(1+z)^4 + \Omega_F y(z, \mathbf{p}) \tag{17}$$

where $\Omega_F = 1 - \Omega_m - \Omega r$, and $\Omega_i = \frac{k^2\rho_{i0}}{3H_0^2}$. In this way, a specific form of $f(T)$ is embodied in the function $y(z, \mathbf{p})$, whose expression is

$$y(z, \mathbf{p}) = \frac{1}{T_0\Omega_F}(f - 2T f_T), \tag{18}$$

where $\mathbf{p}$ stands for the parameters in different forms of $f(T)$ theory.

2.2 Specific $f(T)$ models

In this subsection we briefly review three specific $f(T)$ models, which have passed basic observational tests [37] and will be further investigated in this paper.

(1) The power-law model [15] (hereafter f_1CDM) assumes that the Lagrangian density $f(T)$ of the theory is the following:

$$f(T) = \alpha(-T)^b \tag{19}$$

where α and b are two model parameters. The distortion parameter b quantifies deviation from the ΛCDM model, whereas the parameter α can be expressed through the Hubble constant and density parameter Ω_{F0} by inserting Eq. (19) into Eq. (17) with the boundary condition $E(z=0) = 1$:

$$\alpha = (6H_0^2)^{1-b}\frac{\Omega_{F0}}{2b-1}, \tag{20}$$

Now Eq. (18) may be rewritten as

$$y(z, b) = E^{2b}(z, b). \tag{21}$$

Depending on the choice of parameter b, this $f(T)$ model can be connected with some popular dark energy models. For $b = 0$, it reduces to the ΛCDM, while it can mimic the Dvali–Gabadadze–Porrati (DGP) model when $b = 1/2$.

(2) The exponential model [39] (hereafter f_2CDM) is characterized by

$$f(T) = \alpha T_0(1 - e^{-p\sqrt{T/T_0}}), \tag{22}$$

where α and p are two dimensionless parameters. Similarly the expressions for α and $y(z, p)$ can also be obtained:

$$\alpha = \frac{\Omega_{F0}}{1 - (1+p)e^{-p}}, \tag{23}$$
$$y(z, p) = \frac{1 - (1 + pE)e^{-pE}}{1 - (1+p)e^{-p}}. \tag{24}$$

This model reduces to the ΛCDM in the limit $p \to +\infty$. By setting $b = 1/p$, Eq. (24) is rewritten as

$$y(z, b) = \frac{1 - \left(1 + \frac{E}{b}\right)e^{-E/b}}{1 - \left(1 + \frac{1}{b}\right)e^{-1/b}}, \tag{25}$$

and ΛCDM is recovered when $b \to 0^+$.

(3) Motivated by the exponential $f(R)$ gravity, the hyperbolic-tangent model [17] (hereafter f_3CDM) arises from the ansatz

$$f(T) = \alpha(-T)^n \tanh\left(\frac{T_0}{T}\right) \tag{26}$$

where α and n are the two model parameters. We obtain the expressions for α and $y(z, \mathbf{p})$ as

$$\alpha = -\frac{\Omega_{F0}(6H_0)^{1-n}}{\left[2\mathrm{sech}^2(1) + (1-2n)\tanh(1)\right]}, \tag{27}$$

$$y(z,n)=E^{2(n-1)}\frac{2\mathrm{sech}^2\left(\frac{1}{E^2}\right)+(1-2n)E^2\tanh\left(\frac{1}{E^2}\right)}{2\mathrm{sech}^2(1)+(1-2n)\tanh(1)}, \tag{28}$$

respectively. Compared with two previous $f(T)$ theories, this $f(T)$ model cannot be reduced to the ΛCDM for any value of its parameters. In addition, in order to have a positive value for ρ_{eff}, the parameter n must be greater than 3/2 [17].

3 Observational data and fitting method

In order to measure the angular-diameter distance, we always turn to objects of known comoving size acting as "standard rulers". In this paper, we will consider a combination of three types of standard rulers using the most recent and significantly improved observations, i.e., the compact radio quasars data from VLBI, baryonic acoustic oscillations (BAO) from the large-scale structure, and the cosmic microwave background (CMB) measurements.

3.1 Quasars data

It is well known that the baryon acoustic oscillations (BAO) peak location is commonly recognized as a fixed comoving ruler of about 100 Mpc. Therefore it has already been used in cosmological studies [30–32]. In the same spirit, as extensively discussed in the literature, compact radio sources (quasars, in particular) constitute another possible class of standard rulers of about 10 pc comoving length. Following the analysis of Gurvits [28], the luminosity and redshift dependence of the linear sizes of quasars can be parametrized as

$$l_m = lL^{\beta}(1+z)^n \tag{29}$$

where β and n are two parameters quantifying the "angular size–redshift" and "angular size–luminosity" relations, respectively. The parameter l is the linear size scaling factor representing the apparent distribution of radio brightness within the core. The data used in this paper were derived from an old 2.29 GHz VLBI survey undertaken by Preston et al. (1985), which contains 613 milliarcsecond ultra-compact radio sources covering the redshift range $0.0035 < z < 3.787$. More recently, Cao et al. [29] presented a method to identify a sub-sample which can serve as a certain class of individual standard rulers in the Universe. According to the optical counterparts and luminosities, the full sample could be divided into three sub-samples: low-luminosity quasars ($L < 10^{27}$ W/Hz), intermediate-luminosity quasars (10^{27} W/Hz $< L < 10^{28}$ W/Hz) and high-luminosity quasars ($L > 10^{28}$W/Hz). The final results showed that only intermediate-luminosity quasars show negligible dependence ($|n| \simeq 10^{-3}$, $\beta \simeq 10^{-4}$), and thus they could be a population of rulers once the characteristic length l is fixed. In our analysis, we will use the observations of 120 intermediate-luminosity quasars covering the redshift range $0.46 < z < 2.80$, while the linear size of this standard ruler is calibrated to $l = 11.03$ pc through a new cosmology-independent technique [29].

The observable quantity in this data set is the angular size of the compact structure in intermediate-luminosity radio quasars, whose theoretical (i.e. determined by the cosmological model) counterpart is

$$\theta_{th}(z) = \frac{l}{D_A(z)} \tag{30}$$

where D_A is the angular-diameter distance at redshift z and the $f(T)$ model parameters $\mathbf{p}$ directly enter the angular-diameter distance through

$$D_A(z;\mathbf{p}) = \frac{3000h^{-1}}{(1+z)}\int_0^z \frac{\mathrm{d}z'}{E(z';\mathbf{p})} \tag{31}$$

where $E(z';\mathbf{p})$ is the dimensionless Hubble parameter and h is the dimensionless Hubble constant. We estimate the $f(T)$ parameters by minimizing the corresponding χ^2 defined as

$$\chi^2_{\mathrm{QSO}}(z;\mathbf{p}) = \sum_{i=1}^{120}\frac{[\theta_{\mathrm{th}}(z_i;\mathbf{p})-\theta_{\mathrm{obs}}(z_i)]^2}{\sigma_\theta(z_i)^2} \tag{32}$$

where $\theta_{\mathrm{obs}}(z_i)$ is the observed value of the angular size and $\sigma_\theta(z_i)$ is the corresponding uncertainty for the ith data point in the sample. In order to properly account for the intrinsic spread in linear sizes and systematics we have added in quadrature 10% uncertainties to the $\sigma_\theta(z_i)$.

3.2 CMB and BAO data

In order to diminish the degeneracy between $f(T)$ model parameters we also used the accurate measurements of BAO and CMB.

The CMB experiments measure the temperature and polarization anisotropy of the cosmic radiation in the early epoch. In general, they are a very important tool for the inference of cosmological-model parameters. In particular, the shift parameter R defined as

$$R = \sqrt{\Omega_m}\int_0^{z_*}\frac{\mathrm{d}z'}{E(z';\mathbf{p})}, \tag{33}$$

where $z_* = 1090.43$ denotes the decoupling redshift, is a convenient quantity for a quick fitting of cosmological-model parameters. The first-year data release of *Planck* reported its value of $R = 1.7499 \pm 0.0088$ [41]. We estimate the model parameters by minimizing the corresponding χ^2

Table 1 Ratios of distances and the so-called dilation scale $D_V(z_{\rm BAO})$ at different redshifts $z_{\rm BAO}$ taken after [30–32] and [40]

z_{BAO}	0.106	0.2	0.35	0.44	0.6	0.73
$\frac{r_s(z_d)}{D_V(z_{BAO})}$	0.336 ± 0.015	0.1905 ± 0.0061	0.1097 ± 0.0036	0.0916 ± 0.0071	0.0726 ± 0.0034	0.0592 ± 0.0032
$\frac{d_A(z_*)}{D_V(z_{BAO})}$ $\frac{r_s(z_d)}{r_s(z_*)}$	32.35 ± 1.45	18.34 ± 0.59	10.56 ± 0.35	8.82 ± 0.68	6.99 ± 0.33	5.70 ± 0.31
$\frac{d_A(z_*)}{D_V(z_{BAO})}$	30.95 ± 1.46	17.55 ± 0.60	10.11 ± 0.37	8.44 ± 0.67	6.69 ± 0.33	5.45 ± 0.31

$$\chi^2_{\rm CMB} = \left(\frac{R - 1.7499}{0.0088}\right)^2. \tag{34}$$

The measurements of baryon acoustic oscillation (BAO) in the large-scale structure power spectrum and CMB angular power spectrum have also been widely used for cosmological applications. In this work we consider the measurements of $\frac{d_A(z*)}{D_V(z_{BAO})}$, where $z*$ is the decoupling time, $d_A(z) = \int_0^z \frac{dz'}{H(z')}$ is the comoving angular-diameter distance, and the dilation scale is given by

$$D_V(z) = \left(d_A(z)^2 \frac{z}{H(z)}\right)^{1/3}. \tag{35}$$

The BAO data are shown in Table 1. Similarly, the corresponding χ^2 for the BAO probes is defined as

$$\chi^2_{BAO} = \sum_{ij} X_i C^{-1}_{ij} X_j, \tag{36}$$

where $X = \frac{d_A^{th}(z*)}{D_V^{th}(z_{BAO})} - \frac{d_A^{obs}(z*)}{D_V^{obs}(z_{BAO})}$ and C^{-1}_{ij} is the inverse covariance matrix given by Ref. [40].

4 Observational constraints

In this section, we determine the model parameters of three $f(T)$ cosmologies through the maximum likelihood method based on χ^2 introduced in previous section using the Markov Chain Monte Carlo (MCMC) method. Our code is based on CosmoMC [42] and we generated eight chains after setting $R - 1 = 0.001$ to guarantee the accuracy of this work.

4.1 f_1CDM model: $f(T) = \alpha(-T)^b$

In the case of the $f(T)$ theory based on $f(T) = \alpha(-T)^b$, different data sets and their combinations led to the marginalized 2D confidence contours presented in Figs. 1, 2. The corresponding marginal 1σ error bars can also be seen in Table 2.

The left panel of Fig. 1 shows the contours obtained from the quasars only and in combination with CMB and BAO. We remark that the quasar data only cannot tightly constrain the model parameters. In order to clearly illustrate the constraint comparison between different data sets, a prior $b > -1$ is applied to the likelihood contours obtained from the quasar data. Quantitatively, the value of the distortion parameter b, which quantifies the deviation from the ΛCDM model varies over the interval [-3, 0.56] within 1σ confidence level. As it is well known, the main evidence for cosmic acceleration came from the other type of distance indicators in cosmology, those probing the luminosity distance, D_L by observing the flux of type Ia supernovae (SN Ia). In order to compare our fits with the results obtained using SN Ia, likelihood contours obtained with the latest Union2.1 compilation [43] consisting of 580 SN Ia data points are also plotted in the right panel of Fig. 1. It is clear that the quasar data could give more stringent constraints than SN Ia, and its constraining power becomes obvious when the large size difference between the samples is taken into consideration. This may happen due to the wider redshift range of the quasars data ($0.46 < z < 2.8$) compared with SN Ia ($0.015 \leq z \leq 1.41$). Moreover, one can clearly see from Fig. 1 that principal axes of confidence regions obtained with SN and quasars are inclined at higher angles, which sustains the hope that careful choice of the quasar sample would eventually provide a complementary probe breaking the degeneracy in the $f(T)$ model parameters. Finally, our method based on the observations of intermediate-luminosity quasars may also contribute to testing the consistency between luminosity and angular-diameter distances [44–46].

With the combined standard ruler data sets of quasars, BAO and CMB, the best-fit value for the parameters are $\Omega_{\rm m} = 0.321 \pm 0.012$ and $b = 0.080 \pm 0.077$ within 68.3% confidence level. For comparison, fitting results from SN+BAO+CMB are also given in Fig. 1. The best-fit value is $\Omega_{\rm m} = 0.297^{+0.015}_{-0.017}$ and $b = -0.12^{+0.17}_{-0.13}$, which is in good agreement with that of the quasar+BAO+CMB data. It is obvious that the quasar data, when combined to CMB and BAO observations, can give more stringent constraints on this $f(T)$ cosmology, which demonstrates the strong constraining power of BAO and CMB on the cosmological parameters. This situation has also been extensively discussed in previous work investigating dark energy scenarios with other astrophysical observations [46–50]. Again, the constraining power of 120 quasar data is comparable to that of 580 SN Ia. On the one hand, the present value of the matter density parameter $\Omega_{\rm m}$ given by quasars is much larger than that derived from other observations. This has been noted by our

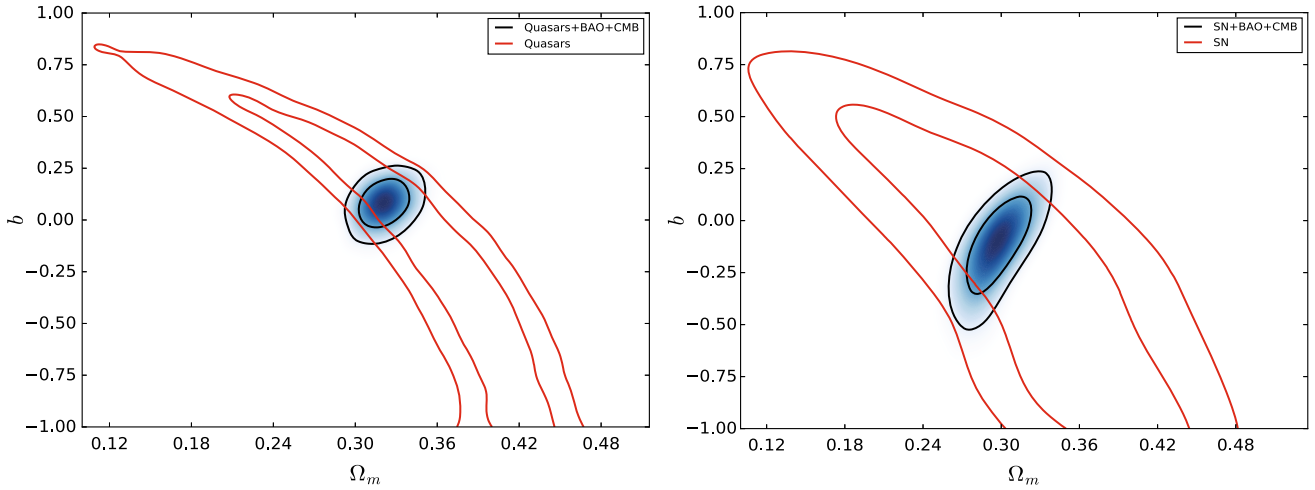

Fig. 1 1σ and 2σ confidence regions for the f_1CDM model. The *red lines* represent contour plot given by quasars (*left panel*) and SN Ia (*right panel*). The *black lines* represent constrained result from the joint analysis of quasars+BAO+CMB (*left panel*) and SN Ia+BAO+CMB (*right panel*)

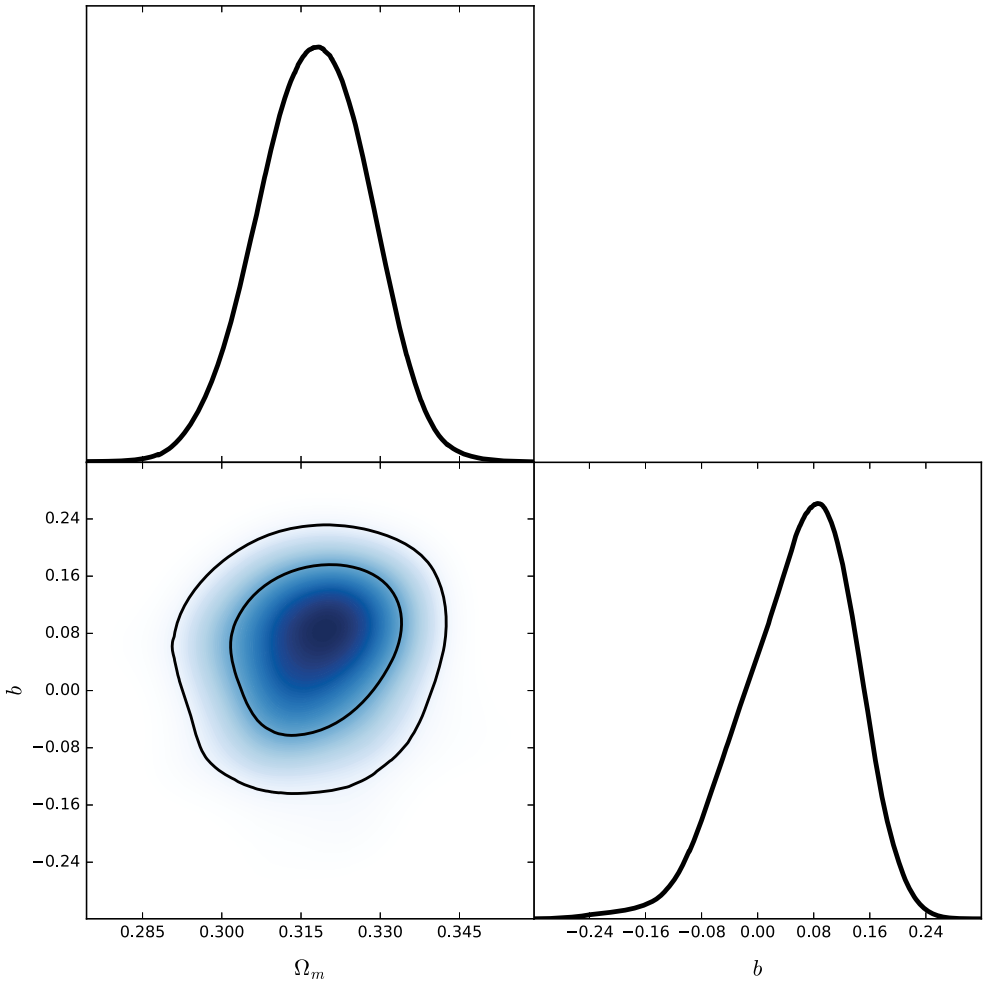

Fig. 2 The 68 and 95% confidence regions for the f_1CDM model, which are constrained by the combined observational data of quasars, SN Ia, BAO and CMB

Table 2 Summary of the best-fit values of parameters for the f_1CDM model with 1σ uncertainties for different observations (OHD is the abbreviation of the observational $H(z)$ data)

Data	Ω_m	b	References
Quasars+BAO+CMB	0.321 ± 0.012	0.080 ± 0.077	This paper
SN Ia+BAO+CMB	$0.297^{+0.015}_{-0.017}$	$-0.12^{+0.17}_{-0.13}$	This paper
Quasars+SN Ia+BAO+CMB	0.317 ± 0.010	$0.057^{+0.091}_{-0.065}$	This paper
OHD+SN Ia+BAO+CMB	$0.2335^{+0.016}_{-0.019}$	$0.05128^{+0.025}_{-0.019}$	[37]
SN Ia+BAO+CMB+dynamical growth data	0.272 ± 0.008	-0.017 ± 0.083	[38]
SN Ia+BAO+varying fundamental constants	0.294 ± 0.022	-0.119 ± 0.185	[51]

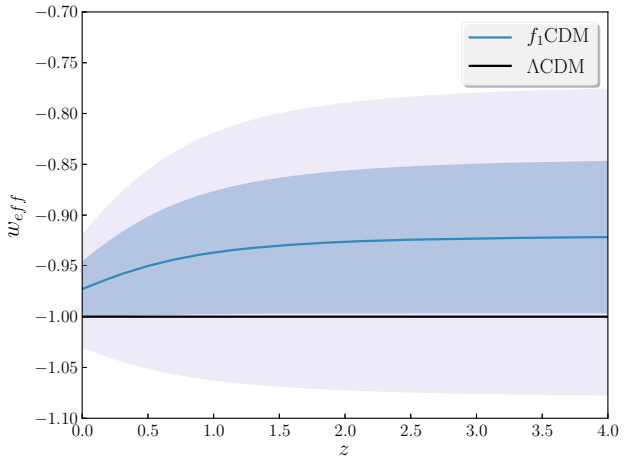

Fig. 3 Evolution of the EoS for ΛCDM (*black line*) and the effective EoS for the f_1CDM model (*blue line*) from the joint analysis quasars+BAO+CMB. 1σ and 2σ uncertainties are, respectively, denoted by *blue* and *gray shades*

previous analysis of Cao et al. [29] and the first-year *Planck* results, in the framework of ΛCDM cosmology. Such a result indicates that quasar data at high redshifts may provide us a different understanding of the parameters describing the components of the Universe. On the other hand, the parameter b, which captures the deviation of $f(T)$ cosmology from the ΛCDM scenario, seems to be vanishing or slightly larger than 0 with the combined quasar+BAO+CMB data. It is interesting to note that ΛCDM is not included at 1σ confidence level ($b = 0.08 \pm 0.077$), this slight deviation from ΛCDM is also consistent with a similar conclusion obtained in Ref. [37] for this f_1CDM model. This tendency can be more clearly seen from Fig. 3, which illustrates the comparison between the effective equation of state for $f(T)$ and the EoS for ΛCDM model at $z \sim 4$, with the best-fitted value as well as the 1σ and 2σ uncertainties derived from the joint data of quasars, BAO and CMB.

The contours constrained with the total combination of quasars+SN Ia+BAO+CMB are presented in Fig. 2, and the best-fit value is $\Omega_{\rm m} = 0.317 \pm 0.010$ and $b = 0.057^{+0.091}_{-0.065}$. The combined data give no stronger constraint, which indicates the constraint ability of quasars data is already very strong, while SN Ia data do not play a leading role in the joint constraint. From the results above, we can see that the ΛCDM model which corresponds to ($b = 0$) is still included within 1σ range. For comparison, in Table 2 we also list alternative constraints obtained by the others using different probes.

4.2 f_2CDM model: $f(T) = \alpha T_0(1 - e^{-p\sqrt{T/T_0}})$

Performing a similar analysis as before, this time with the other $f(T)$ model in which ΛCDM is also nested, namely, $f(T) = \alpha T_0(1 - e^{-p\sqrt{T/T_0}})$, we made the same comparison as f_1CDM discussed above, i.e. quasars vs. SN Ia and quasars+BAO+CMB vs. SN Ia+BAO+CMB. The results are presented in Fig. 4 and the estimated cosmic parameters are briefly summarized in Table 3. It is apparent that the quasars data exhibit similar constraining power as in the case of f_1CDM model, which implies that the constraint ability of 120 quasar data can be comparable to that of 580 SN Ia. By fitting the f_2CDM model to quasars+BAO+CMB, we obtain $\Omega_{\rm m} = 0.319 \pm 0.011$ and $b < 0.268$ (let us recall that here we introduced $b = 1/p$).

With the combined data set of quasars+SN Ia+BAO+CMB, we also get the marginalized 1σ constraints of the parameters as $\Omega_{\rm m} = 0.319^{+0.010}_{-0.011}$ and $b < 0.224$. The marginalized 1σ and 2σ contours of each parameter are presented in Fig. 6. In Table 3, the best-fit parameters and their 1σ uncertainties for three data sets are displayed. As previously the results from the others using different probes are shown for comparison. Obviously, the present matter density parameter $\Omega_{\rm m}$ fitted by quasars is larger than given by other observations. The parameter b quantifying the deviation from the ΛCDM scenario, tends to be zero for all of observations listed in Table 3, which results in that the exponential gravity is practically indistinguishable from ΛCDM. As can be seen from the results presented in Fig. 5, even at 2σ confidence level, the effective EoS of f_2CDM model from the joint analysis of quasars, BAO and CMB agrees very well with that of ΛCDM at $z \sim 4$, which strongly indicates the consistency between the two types of cosmological models at much higher redshifts.

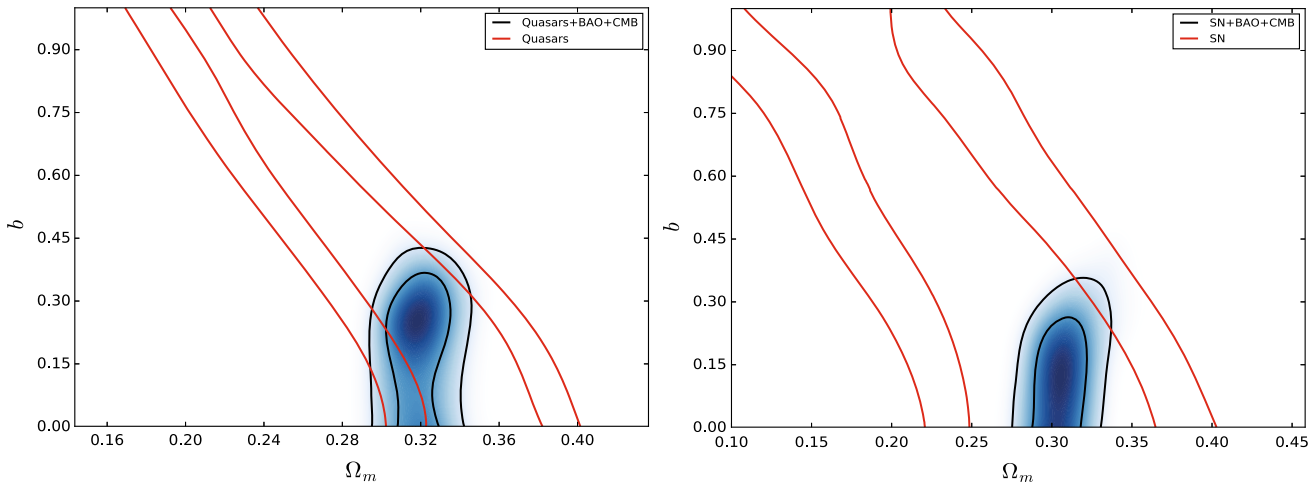

Fig. 4 1σ and 2σ confidence regions for the f_2CDM model. The *red lines* represent contour plot given by quasars (*left panel*) and SN Ia (*right panel*). The *black lines* represent constrained result from the joint analysis quasars+BAO+CMB (*left panel*) and SN Ia+BAO+CMB (*right panel*)

Table 3 Summary of the best-fit values of parameters for the f_2CDM model with 1σ uncertainties for different observations

Data	Ω_m	b	References
Quasars+BAO+CMB	0.319 ± 0.011	$b < 0.268$	This paper
SN Ia+BAO+CMB	0.307 ± 0.013	$b < 0.186$	This paper
Quasars+SN Ia+BAO+CMB	$0.319^{+0.010}_{-0.011}$	$b < 0.224$	This paper
OHD+SN Ia+BAO+CMB	$0.2784^{+0.0097}_{-0.019}$	$0.1325^{+0.043}_{-0.13}$	[37]
SN Ia+BAO+CMB+dynamical growth data	0.272 ± 0.004	0.121 ± 0.184	[38]
SN Ia+BAO+varying fundamental constants	0.283 ± 0.018	0.024 ± 0.08	[51]

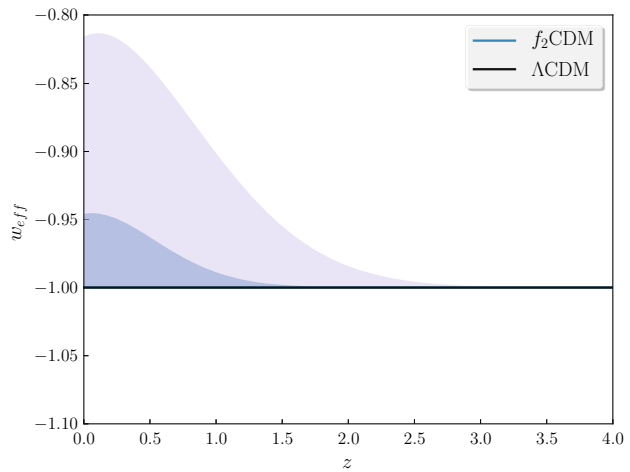

Fig. 5 Evolution of the EoS for ΛCDM and the effective EoS for the f_2CDM model from the joint analysis quasars+BAO+CMB

4.3 f_3CDM model: $f(T) = \alpha(-T)^n \tanh\left(\frac{T_0}{T}\right)$

Now we will discuss the third version of $f(T)$ cosmology which is truly an alternative to the ΛCDM since the concordance cosmological model cannot be recovered as a limiting case of f_3CDM model. Consequently, the parameter n does not characterize the deviation from ΛCDM.

In Fig. 7 we present contour plots of f_3CDM model parameters fitted to four different probes, namely quasars, SN Ia, quasars+BAO+CMB, and SN Ia+BAO+CMB. As we can see, the quasar data provide more stringent constraints than SN Ia, which indicates that the constraining ability of quasar data can be comparable to or better than that of SN Ia at least in this particular model. In Fig. 8 we show the contour plots for the combination of all data sets quasars+SN Ia+BAO+CMB. Additionally, in Table 4 we summarize the best-fit values for the three combined data sets, respectively. Table 4 also includes the best-fit values and their 68% confidence levels for the previous results from the literature. Similar to the cases of f_1CDM model and f_2CDM model, the present matter density parameter Ω_m implied by quasars is larger than that given by other observations. Concerning the value of the parameter n, its value constrained by all of the current observations satisfies the condition $n > 3/2$, which is necessary to achieve the cosmic acceleration in the framework of f_3CDM.

In Fig. 9 we show the evolution of the effective equation of state for f_3CDM model as a function of redshift, concerning the best-fitted value with the 1σ and 2σ uncertainties from the joint data of quasars, BAO and CMB. In particular, we find that the value of n obtained with quasars suggests that

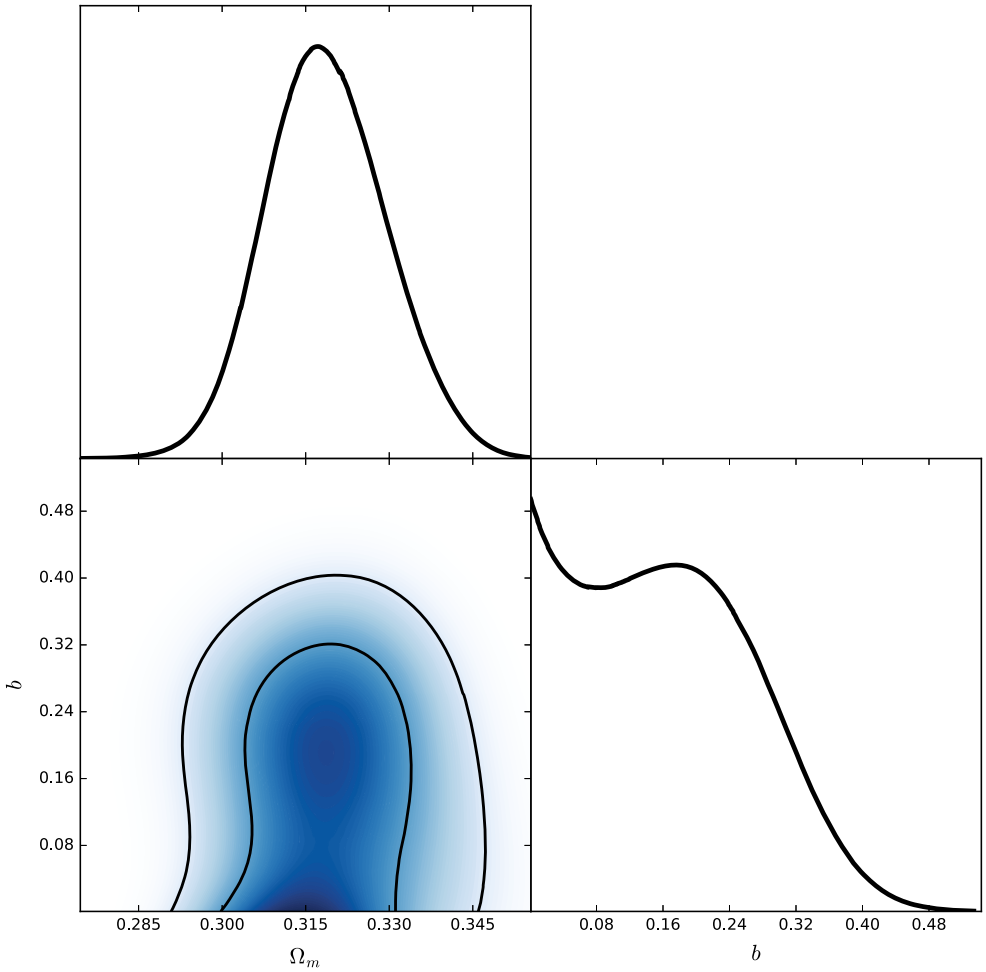

Fig. 6 The 68 and 95% confidence regions for the f_2CDM model, which are constrained by the combined observational data of quasars, SN Ia, BAO and CMB

the effective equation of state crosses the phantom divide line at lower redshifts [17].

4.4 Model selection

In order to make a good comparison between different models or decide which model is preferred by the observational data, we will use two standard information criteria, namely the Akaike Information Criterion (AIC) [53] and the Bayesian Information Criterion (BIC) [54] to study competing models. The above two information criteria are, respectively, defined as

$$\mathrm{AIC} = -2\ln\mathcal{L} + 2k \tag{37}$$

and

$$\mathrm{BIC} = -2\ln\mathcal{L} + k\ln N, \tag{38}$$

where $\mathcal{L} = \exp(-\chi^2_{\mathrm{min}}/2)$, k represents the number of free parameters in the model and N is the sample size used in the statistical analysis. In addition, we introduce the ratio of χ^2_{min} to the degrees of freedom (d.o.f.), $\chi^2_{\mathrm{min}}/d.o.f.$, to judge the quality of observational data set.

In Table 5, we list the values of AIC, BIC and χ^2_{min}/d.o.f. for different models from the joint analysis quasar+BAO +CMB and SN Ia+BAO+CMB. It is obvious that both the AIC and the BIC criteria support ΛCDM to be the best cosmological model consistent with the available observations, since the IC value it yields is the smallest. Concerning the ranking of the three $f(T)$ models, AIC and BIC criteria tend to provide the same conclusions as follows. The f_2CDM model performs the best in explaining the current data, which can be clearly seen from the similarity between f_2CDM and ΛCDM shown in Fig. 5. Then next after f_2CDM is the f_1CDM model, which can also reduce to the ΛCDM model and its best-fit parameters indeed do so. The worst

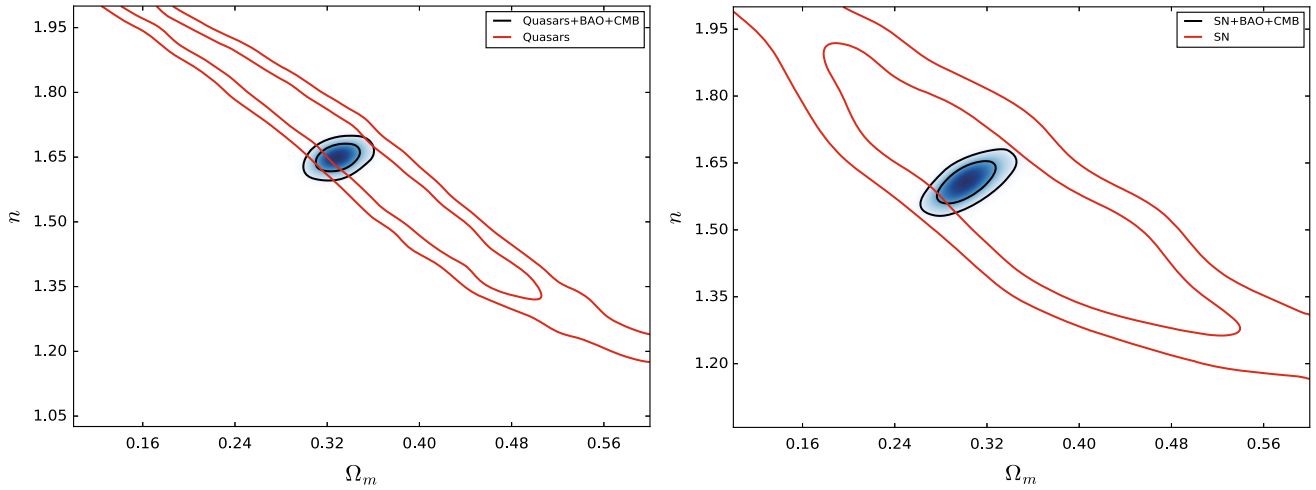

Fig. 7 1σ and 2σ confidence regions for the f_3CDM model. The *red lines* represent contour plot given by quasars (*left panel*) and SN Ia (*right panel*). The *black lines* represent constrained result from the joint analysis quasars+BAO+CMB (*left panel*) and SN Ia+BAO+CMB (*right panel*)

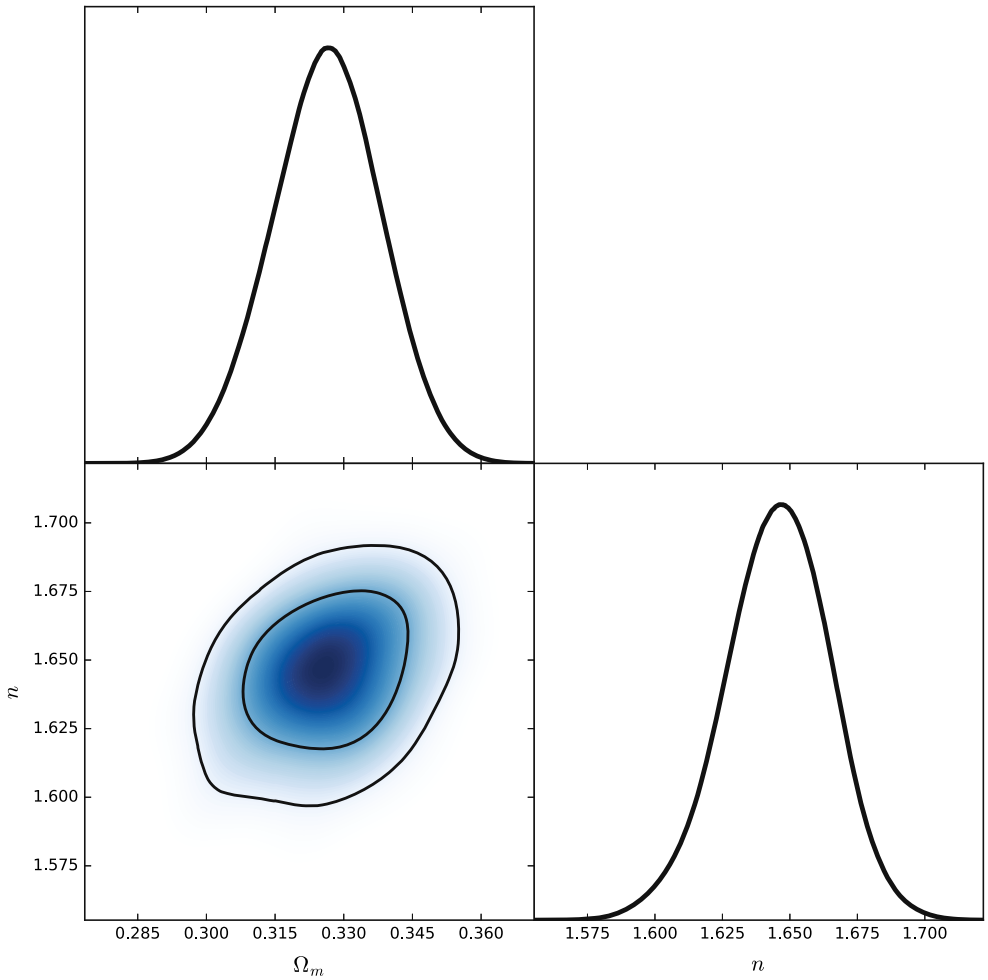

Fig. 8 The 68 and 95% confidence regions for the f_3CDM model, which are constrained by the combined observational data of quasars, SN Ia, BAO and CMB

Table 4 Summary of the best-fit values of parameters for the f_3CDM model with 1σ uncertainties for different observations

Data	Ω_m	n	References
Quasars+BAO+CMB	0.329 ± 0.011	1.649 ± 0.021	This paper
SN Ia+BAO+CMB	0.303 ± 0.017	1.607 ± 0.031	This paper
Quasars+SN Ia+BAO+CMB	0.326 ± 0.012	$1.645^{+0.020}_{-0.018}$	This paper
GRB+OHD+SN Ia+BAO+CMB	$0.286^{+0.013}_{-0.012}$	$1.616^{+0.02}_{-0.035}$	[52]

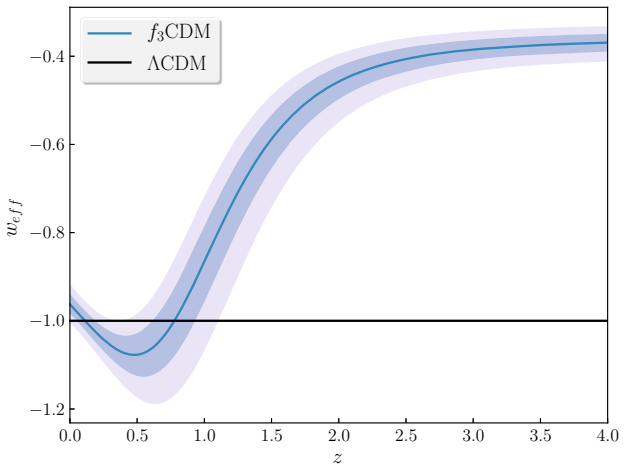

Fig. 9 Evolution of the EoS for ΛCDM and the effective EoS for the f_3CDM model from the joint analysis quasars+BAO+CMB

model according to the AIC and BIC criteria is f_3CDM, which is unable to provide a good fit to the data and cannot nest ΛCDM.

5 Conclusions and discussions

As an interesting approach to modifying gravity, $f(T)$ theory based on the concept of teleparallel gravity, was proposed to explain the accelerated expansion of the Universe without the need of dark energy. In this paper, we have used the recently released sample of VLBI observations of the compact structure in 120 intermediate-luminosity quasars ($0.46 < z < 2.80$) to get the constraints on the viable and most popular $f(T)$ gravity models. The statistical linear sizes of these quasars observed at 2.29 GHz show negligible dependence on redshifts and intrinsic luminosity, and thus represent a fixed comoving length of the standard ruler. Therefore, the other motivation of this work was to investigate the constraining ability of quasar data in the context of $f(T)$ models. In particular, we have considered three $f(T)$ models with two parameters, out of which two could nest the concordance ΛCDM model and we quantified their deviation from ΛCDM cosmology through a single parameter b. For the third $f(T)$ cosmology which cannot be directly reduced to ΛCDM, we discussed the possibility for the effective equation of state to cross the phantom divide line.

In our investigation we have used (i) the very recently released "angular size–redshift" data sets of 120 intermediate-luminosity quasars in the redshift range $0.46 < z < 2.76$, (ii) the cosmic microwave background and baryon acoustic oscillation data points. Meanwhile, in order to compare our fits obtained with 120 quasars (standard rulers), to the similar constraints obtained with the Union2.1 compilation consisting of 580 SN Ia data points (standard candles) we also carried out respective analysis based on SNIa data. Here we summarize our main conclusions in more detail:

- For all of the three the $f(T)$ models, all of the fitting results show that the quasar data ($N = 120$) could provide more stringent constraints than the Union2.1 SN Ia data ($N = 580$). This may be associated with the wider redshift range covered by the quasar data ($0.46 < z < 2.8$) compared with SN Ia ($0.015 \leq z \leq 1.41$). The constraining power of the former becomes obvious when the large size difference between the samples is taken into consideration. Moreover, one can clearly see that principal axes of confidence regions obtained with SN and quasars are inclined at higher angles, which sustains the hope that a careful choice of the quasar sam-

Table 5 Summary of the AIC and BIC values for different models obtained from the combined quasar+BAO+CMB data and the combined SN Ia +BAO+CMB data

Model	Quasar+BAO+CMB					SN Ia+BAO+CMB				
	AIC	ΔAIC	BIC	ΔBIC	$\chi^2_{\min}$/d.o.f.	AIC	ΔAIC	BIC	ΔBIC	$\chi^2_{\min}$/d.o.f.
ΛCDM	613.78	0	616.62	0	4.80	550.87	0	555.24	0	0.95
f_1CDM	615.46	1.68	621.15	4.53	4.81	552.94	2.07	561.69	6.45	0.95
f_2CDM	615.32	1.54	621.01	4.39	4.81	552.83	1.96	561.58	6.34	0.95
f_3CDM	616.91	3.13	622.60	5.98	4.83	553.01	2.14	561.76	6.52	0.95

ple would eventually provide a complementary probe breaking the degeneracy in the $f(T)$ model parameters. Our method based on the observations of intermediate-luminosity quasars may also contribute to testing the consistency between luminosity and angular-diameter distances.

- The present value of the matter density parameter $\Omega_{\rm m}$ implied by quasars is much larger than that derived from other observations, which has been noted by our previous analysis and the first-year *Planck* results, in the framework of ΛCDM cosmology. Such a result indicates that quasar data at high redshifts may provide us with a different understanding of the components in the Universe.
- For f_1CDM and f_2CDM models, deviation from ΛCDM cosmology is also allowed in the obtained confidence level, although the best-fit value is very close to its ΛCDM one. It is interesting in the present work to note that ΛCDM is not included at 1σ confidence level for the power-law model f_1CDM model, this slight deviation from ΛCDM is also consistent with a similar conclusion obtained in the previous observational studies on $f(T)$ gravity. In the framework of f_3CDM, the value of n constrained by all of the current observations satisfies the limit of $n > 3/2$, which is necessary to achieve the cosmic acceleration. Moreover, we find that the value of n obtained with quasars suggests that the effective equation of state can cross the phantom divide line at lower redshifts.
- The information criteria (AIC and BIC) demonstrate that, compared with other three $f(T)$ scenarios considered in this paper, the cosmological constant model is still the best cosmological model consistent with the available observations. Concerning the ranking of the $f(T)$ cosmologies, the f_2 CDM model performs the best in explaining the current data, while the f_3 CDM model gets the smallest support and cannot nest the concordance ΛCDM model.
- In summary, using for the recently released quasar data acting as a new source of standard rulers, we were able to set more stringent limits on the viable and most used $f(T)$ gravity models. Our results highlight the importance of quasar measurements to provide additional information of various candidates for modified gravity, especially the possible deviation from ΛCDM cosmology. More importantly, given the usefulness of this angular size data in pinning down parameter values, we also anticipate that near-future quasar observations will provide significantly more restrictive constraints on other torsional modified gravity theories [11,55,56].

Acknowledgements This work was supported by the National Key Research and Development Program of China under Grants No. 2017YFA0402603, the Ministry of Science and Technology National Basic Science Program (Project 973) under Grants No. 2014CB845806, the National Natural Science Foundation of China under Grant Nos. 11503001, 11373014 and 11690023, the Fundamental Research Funds for the Central Universities and Scientific Research Foundation of Beijing Normal University, China Postdoctoral Science Foundation under Grant No. 2015T80052, and the Opening Project of Key Laboratory of Computational Astrophysics, National Astronomical Observatories, Chinese Academy of Sciences. This research was also partly supported by the Poland–China Scientific & Technological Cooperation Committee Project No. 35-4. M.B. obtained approval of foreign talent introducing project in China and gained special fund support of the foreign knowledge introducing project.

References

1. A. Riess et al., Astron. J. **116**, 1009 (1998)
2. M. Tegmark, M. Strauss, M. Blanton et al., Phys. Rev. D **69**(10), 103501 (2004)
3. D. Spergel et al., Astrophys. J. Suppl. **148**(175), 170 (2003)
4. R. Caldwell, E.V. Linder, Phys. Rev. Lett. **95**, 141301 (2005). doi:10.1103/PhysRevLett.95.141301
5. I. Zlatev, L.M. Wang, P.J. Steinhardt, Phys. Rev. Lett. **82**, 896 (1999). doi:10.1103/PhysRevLett.82.896
6. S. Tsujikawa, Class. Quantum Gravity **30**, 214003 (2013). doi:10.1088/0264-9381/30/21/214003
7. E. Barboza Jr., J. Alcaniz, Z.H. Zhu, R. Silva, Phys. Rev. D **80**(4), 043521 (2009)
8. I. Maor, R. Brustein, P.J. Steinhardt, Phys. Rev. Lett. **86**(1), 6 (2001)
9. E.V. Linder, Phys. Rev. Lett. **90**(9), 091301 (2003)
10. H. Wei, X.P. Yan, Y.N. Zhou, JCAP **1401**, 045 (2014). doi:10.1088/1475-7516/2014/01/045
11. B. Boisseau, G. Esposito-Farese, D. Polarski, A.A. Starobinsky, Phys. Rev. Lett. **85**(11), 2236 (2000)
12. G. Dvali, G. Gabadadze, M. Porrati, Phys. Lett. B **484**(1), 112 (2000)
13. T. Chiba, Phys. Lett. B **575**(1), 1 (2003)
14. S. Nojiri, S.D. Odintsov, Phys. Lett. B **631**(1), 1 (2005)
15. G.R. Bengochea, R. Ferraro, Phys. Rev. D **79**(12), 124019 (2009)
16. C. Xu, E.N. Saridakis, G. Leon, J. Cosmol. Astropart. Phys. **1207**(07), 005 (2012)
17. P. Wu, H. Yu, Eur. Phys. J. C **71**(2), 1 (2011)
18. Y.F. Cai, S. Capozziello, M. De Laurentis, E.N. Saridakis, arXiv preprint arXiv:1511.07586 (2015)
19. J.Z. Qi, R.J. Yang, M.J. Zhang, W.B. Liu, Res. Astron. Astrophys. **16**(2), 002 (2016)
20. R.J. Yang, Eur. Phys. J. C **71**(11), 1 (2011)
21. S. Cao, M. Biesiada, J. Jackson, X. Zheng, Z.H. Zhu, arXiv preprint arXiv:1609.08748 (2016)
22. J. Jackson, M. Dodgson, Mon. Not. R. Astron. Soc. **285**(4), 806 (1997)
23. R. Vishwakarma, Class. Quantum Gravity **18**(7), 1159 (2001)
24. J. Lima, J. Alcaniz, Astrophys. J. **566**(1), 15 (2002)
25. Z.H. Zhu, M.K. Fujimoto, Astrophys. J. **581**(1), 1 (2002)
26. G. Chen, B. Ratra, Astrophys. J. **582**(2), 586 (2003)
27. K. Kellermann, Nature **361**(6408), 134 (1993)
28. L. Gurvits, Astrophys. J. **425**, 442 (1994)

29. S. Cao, X.G. Zheng, M. Biesiada, J.Z. Qi, Y. Chen, Z.H. Zhu, Astron. Astrophys (2017). doi:10.1051/0004-6361/201730551
30. W.J. Percival, B.A. Reid, D.J. Eisenstein, N.A. Bahcall, T. Budavari, J.A. Frieman, M. Fukugita, J.E. Gunn, Ž. Ivezić, G.R. Knapp et al., Mon. Not. R. Astron. Soc. **401**(4), 2148 (2010)
31. C. Blake, E.A. Kazin, F. Beutler, T.M. Davis, D. Parkinson, S. Brough, M. Colless, C. Contreras, W. Couch, S. Croom et al., Mon. Not. R. Astron. Soc. **418**(3), 1707 (2011)
32. F. Beutler, C. Blake, M. Colless, D.H. Jones, L. Staveley-Smith, L. Campbell, Q. Parker, W. Saunders, F. Watson, Mon. Not. R. Astron. Soc. **416**(4), 3017 (2011)
33. M. Bonamente, M. Joy, S.J. Laroque, J.E. Carlstrom, E.D. Reese, K.S. Dawson, Astrophys. J. **647**(1), 25 (2006)
34. M. Biesiada, B. Malec, A. Piorkowska, Res. Astron. Astrophys. **11**(6), 641 (2011)
35. S. Cao, Y. Pan, M. Biesiada, W. Godlowski, Z. Zhu, J. Cosmol. Astropart. Phys. **2012**(3), 16 (2012)
36. S. Cao, M. Biesiada, R. Gavazzi, A. Piorkowska, Z. Zhu, Astrophys. J. **806**(2), 185 (2015)
37. R.C. Nunes, S. Pan, E.N. Saridakis, J. Cosmol. Astropart. Phys. **2016**(08), 011 (2016)
38. S. Nesseris, S. Basilakos, E. Saridakis, L. Perivolaropoulos, Phys. Rev. D **88**(10), 103010 (2013)
39. E.V. Linder, Phys. Rev. D **81**(12), 127301 (2010)
40. R. Giostri, M.V. dos Santos, I. Waga, R. Reis, M. Calvao, B. Lago, J. Cosmol. Astropart. Phys. **2012**(03), 027 (2012)
41. P. Ade, N. Aghanim, C. Armitage-Caplan, M. Arnaud, M. Ashdown, F. Atrio-Barandela, J. Aumont, C. Baccigalupi, A. Banday, R. Barreiro et al., Astron. Astrophys. **571**, A16 (2014)
42. A. Lewis, S.L. Bridle, Phys. Rev. D **66**(10), 103511 (2002)
43. N. Suzuki, D. Rubin, C. Lidman, G. Aldering, R. Amanullah, K. Barbary, L. Barrientos, J. Botyanszki, M. Brodwin, N. Connolly et al., Astrophys. J. **746**(1), 85 (2012)
44. S. Cao, Z. Zhu, Sci. China Phys. Mech. Astron. **54**(12), 2260 (2011)
45. S. Cao, N. Liang, Res. Astron. Astrophys. **11**(10), 1199 (2011)
46. S. Cao, Z.H. Zhu, Phys. Rev. D **90**(8), 083006 (2014)
47. S. Cao, N. Liang, Z. Zhu, Mon. Not. R. Astron. Soc. **416**(2), 1099 (2010)
48. S. Cao, N. Liang, Int. J. Mod. Phys. D **22**(14), 1350082 (2011)
49. S. Cao, Z. Zhu, Astron. Astrophys. **538**, A61 (2011)
50. Y. Pan, S. Cao, Y. Gong, K. Liao, Z. Zhu, Phys. Lett. B **718**(3), 699 (2012)
51. R.C. Nunes, A. Bonilla, S. Pan, E.N. Saridakis, arXiv preprint arXiv:1608.01960 (2016)
52. V.F. Cardone, N. Radicella, S. Camera, Phys. Rev. D **85**(12), 124007 (2012)
53. H. Akaike, IEEE Trans. Autom. Control **19**(6), 716 (1974)
54. G. Schwarz, Ann. Stat. **6**(2), 461 (1978)
55. G. Kofinas, E.N. Saridakis, Phys. Rev. D **90**(8), 084045 (2014)
56. T. Harko, F.S. Lobo, G. Otalora, E.N. Saridakis, Phys. Rev. D **89**(12), 124036 (2014)